Atlantic Multidecadal Variability as a Modulator of Precipitation Variability in the Southwest United States

DONG EUN LEE AND MINGFANG TING

Lamont-Doherty Earth Observatory, Columbia University, Palisades, New York

NICOLAS VIGAUD

International Research Institute for Climate and Society, Columbia University, Palisades, New York

YOCHANAN KUSHNIR

Lamont-Doherty Earth Observatory, Columbia University, Palisades, New York

ANTHONY G. BARNSTON

International Research Institute for Climate and Society, Columbia University, Palisades, New York

(Manuscript received 2 June 2017, in final form 12 April 2018)

ABSTRACT

Two independent atmospheric general circulation models reveal that the positive (negative) phase of Atlantic multidecadal variability (AMV) can reduce (amplify) the variance of the shorter time-scale (e.g., ENSO related) precipitation fluctuations in the United States, especially in the Southwest, as well as decrease (increase) the long-term seasonal mean precipitation for the cold season. The variance is modulated because of changes in 1) dry day frequency and 2) maximum daily rainfall intensity. With positive AMV forcing, the upper-level warming originating from the increased precipitation over the tropical Atlantic Ocean changes the mean vertical thermal structure over the United States continent to a profile less favorable for rain-inducing upward motions. In addition, a northerly low-level dry advection associated with the local overturning leaves less available column moisture for condensation and precipitation. The opposite conditions occur during cold AMV periods.

1. Introduction

Winter precipitation in the Southwest United States (SW-US) is of great importance as it affects the soil moisture accumulation for vegetation and reservoir levels for local agriculture into the following spring (Notaro et al. 2010). In the desert lands in the SW-US, a peak of low-intensity rainfall occurs in the cold season because of large-scale weather systems, while a peak of higher-intensity rainfall takes place in the warm season under the influences of convective storms and the North American monsoon. In the mountain area, precipitation is primarily driven by orography, and is evenly distributed through the year. Typically, winter precipitation in the SW-US is widespread, is of low to moderate intensity, and can persist for a few days. Occasional cyclones traveling northward from the tropical Pacific can deliver substantial and multiday precipitation as well (Sheppard et al. 2002).

The severe precipitation deficit in the SW-US in recent decades has had seriously adverse socioeconomic impacts (Howitt et al. 2014). The recent long-lasting drought in SW-US has been attributed largely to the relative absence of strong El Niños during the last two decades and an early expression of anthropogenic warming (Seager et al. 2015). The strong El Niño event of 2015/16 was expected to provide relief to the drought stricken SW-US, but it failed. This motivated the examination of the sources of uncertainty in the ENSO–SW-US precipitation relationship. Recent studies point to random internal variability as having altered the typical circulation pattern associated with El Niño (Seager and Hoerling 2014; Seager et al. 2015; Schubert et al. 2016). Other influences, such as the Arctic sea ice

Corresponding author: Dong Eun Lee, dlee@ldeo.columbia.edu

DOI: 10.1175/JCLI-D-17-0372.1

anomaly (Sewall and Sloan 2004) or the state of the tropical Atlantic SST, could be relevant (Schubert et al. 2004; Kushnir et al. 2010; Seager and Hoerling 2014). Other studies alluded to the detailed structure of the SST anomalies, such as the amplitude and longitudinal position of the El Niño–Southern Oscillation (ENSO) sea surface temperature (SST) anomalies, which have been considered essential in determining the impact over the North American surface climate (Guo et al. 2017; Jong et al. 2018).

Another aspect that may contribute to uncertainties in the ENSO–North American climate teleconnection, particularly in terms of precipitation, is the slowly varying large-scale environment caused by decadal or longer time-scale impacts from the oceans. The process leading to continental precipitation is nonlinear, requiring an air parcel to be lifted beyond the lifted condensation level; thus, precipitation is linked to both upward motion and available water vapor. It is therefore important to explore the decadal and longer-term variability of the background state and whether it may impact the subseasonal to interannual precipitation variability associated with phenomena such as the Madden–Julian oscillation (MJO) and ENSO.

Atlantic multidecadal variability (AMV), which refers to the low-frequency variation of basinwide SST extending from the subpolar North Atlantic into the tropics in what resembles a horseshoe pattern (Fig. 1a), has been implicated as a possible factor that can exert a long-term impact on precipitation variability in the continental United States (Enfield et al. 2001; Sutton and Hodson 2005). Several previous studies have explored the AMV modulation of the ENSO impact over North America (Enfield et al. 2001; Rogers and Coleman 2003; Mo et al. 2009; Hu et al. 2011; Hu and Feng 2012). Based on a coordinated modeling study, Mo et al. (2009) suggested that warm season precipitation responds asymmetrically to ENSO under the influence of AMV, although there were considerable model-to-model disagreements in the rainfall response to ENSO, which could substantially interfere with the ensemble mean ENSO asymmetry associated with AMV. In the Great Plains, the modeled precipitation contrast between El Niño and La Niña cases was amplified during a positive AMV during summer [see Table 1 in Hu and Feng (2012)]. Thus, in these previous studies, the AMV appears as a modulator to the continental precipitation response to any source of shorter-term climate variability, particularly ENSO.

Although the mean impact of AMV on North American precipitation has been widely recognized (e.g., Enfield et al. 2001; McCabe et al. 2004; Sutton and Hodson 2005; Knight et al. 2006; Ting et al. 2009, 2011), the physical mechanisms underlying its role in modulating precipitation responses to climate variations on shorter time scales is not fully understood. We hypothesize that the long-lasting impact of AMV on the background state can further influence the characteristics of the local precipitation response to shorter-term disturbances over the continental United States, including ENSO and internal atmospheric variability. To identify how and where AMV exerts its effects, we designed atmospheric general circulation model (AGCM) experiments forced with the typical AMV SST pattern added and subtracted from the climatology. As our focus is on the SW-US, where winter is the wettest season, we focus on the response during that season. Furthermore, we investigate the general causes of the modulation on short-term precipitation variability regardless of whether it is SST-forced or driven by internal atmospheric variability.

This paper is organized as follows: in section 2 we introduce the data used in this study and the design of the experiments, and in section 3 we explore the response associated with different phases of AMV in observations and in the model experiments with globally prescribed historical SST. Then in section 4 we discuss the impact driven purely by the AMV SST anomalies. Final discussion and conclusions follow in section 5.

2. Data, models, and method

a. Model description

Two AGCMs—the National Center for Atmospheric Research (NCAR) Community Atmosphere Model, version 5.3 (CAM5) and the Max Planck Institute for Meteorology European Centre Hamburg Model, version 5 (ECHAM5)—are used in this study. CAM5 is the atmospheric component of the Community Earth System Model, version 1.2 (CESM; Neale et al. 2013). It uses an Eulerian dynamical core with T42 spectral horizontal grid and 30 sigma-pressure hybrid vertical levels. It is coupled to the Community Land Model, version 4 (CLM4; Oleson et al. 2013) and the Community Ice Code, version 4 (CICE4; Holland et al. 2012) with prescribed sea ice concentration, following the F_2000_CAM5 component set. More detail can be found in Neale et al. (2013). The ECHAM5 is a spectral model, truncated at T42 horizontal resolution and vertically discretized at 19 sigma-pressure hybrid levels (Simmons and Burridge 1981). Land surface processes for temperature and moisture are iterated interactively with the atmospheric model (Schulz 2001). Sea surface temperature and sea ice concentration are prescribed with the monthly observations. A complete description of the model can be found in Roeckner et al. (2003).

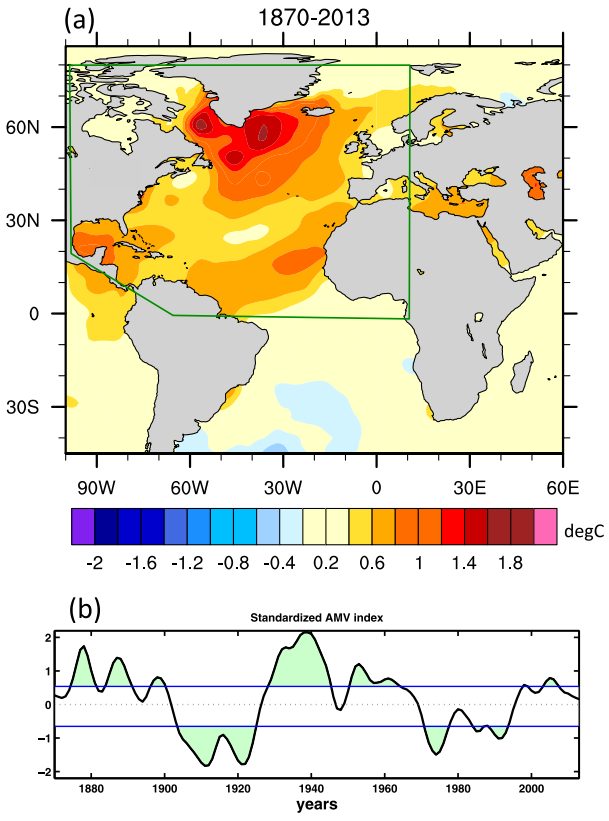

FIG. 1. (a) SST anomaly pattern in the North Atlantic prescribed in the idealized experiments. It is made from linear regression coefficients, multiplied by a factor of 2.5, (b) with the standardized AMV index by Ting et al. (2009) shown. The negative phase is represented by the same anomalies multiplied by −1. The enclosed area in green indicates the location where SST anomalies are prescribed for the idealized experiments. The upper tercile and lower tercile values of the AMV index are marked by the blue horizontal lines in (b), which define the years filled in green shading that represent the AMV+ and AMV− years for the composite analysis.

b. Model experiments

CAM5-GOGA (Guo et al. 2017; Pomposi et al. 2016) is a 16-member ensemble of the so-called Global Ocean Global Atmosphere (GOGA) experiment forced by observed historical global, monthly SST anomalies. In this case, SST forcing data are taken from the Hadley Centre Sea Ice and Sea Surface Temperature, version 2 (HadISSTv2; Titchner and Rayner 2014), spanning the years 1856 to 2014. Sea ice concentration varies with time according to the historical record depicted in HadISSTv2. Greenhouse gas concentrations are kept at the year 2000 value and there is no time-varying external radiative forcing. The model integration begins from 16 slightly different initial conditions to facilitate the generation of independent samples that reflect the free, internal atmospheric variability. A 16-member ensemble GOGA experiment with the same boundary condition with CAM5-GOGA is also conducted with ECHAM5 (ECHAM5-GOGA) for comparison and assessment of the robustness of the results.

TABLE 1. List of the AGCM experiments used in this study.

	CAM5	ECHAM5
GOGA	16 ensemble 1856–2016	16 ensemble 1930–2013
AMV+ CTRL AMV−	60 annual cycles	60 annual cycles

Idealized AMV experiments are conducted with the two GCMs, CAM5, and ECHAM5. Both models are integrated through 60 annual cycles with prescribed AMV anomalies added to the SST climatology, which is the average seasonal cycle in the base period of 1930–2000 from ERSSTv4 (Huang et al. 2015). We considered two opposite AMV phases confined within the North Atlantic: a positive phase (AMV+) and negative phase (AMV−). A neutral case (CTRL) is also considered. The AMV SST pattern is derived from the linear regression on the standardized AMV index defined by Ting et al. (2009). To obtain a robust response to the AMV, the regression pattern is multiplied by a factor of 2.5. The green line in Fig. 1a outlines the domain of the whole North Atlantic SST forcing. We also considered the impact of three regional sectors of the AMV: the whole North Atlantic, the extratropical North Atlantic north of 45°N, and the tropical North Atlantic south of 45°N. The list of all the experiments is provided in Table 1.

c. Observed data

The SST data used for generating the AMV pattern in the North Atlantic are taken from the Extended Reconstructed SST, version 4 (ERSSTv4) dataset (Huang et al. 2015) during 1870–2013. The AMV index is obtained following Ting et al. (2009, 2011). First, the radiatively forced component is obtained by applying a signal-to-noise-maximizing EOF (Allen and Smith 1997) to the low-pass-filtered global SST of multimodel and multiensemble CMIP3 simulations. Then, linear regression of the observed global SST onto the principal component of the leading forced mode is used to remove the global warming footprint from the observed SST. After filtering out the forced component, the AMV index is obtained as the residual of the observed North Atlantic basinwide average. Finally, the observed SST pattern without the forced component in the North Atlantic is obtained using linear regression onto the AMV index (Fig. 1a). The typical SST pattern of AMV

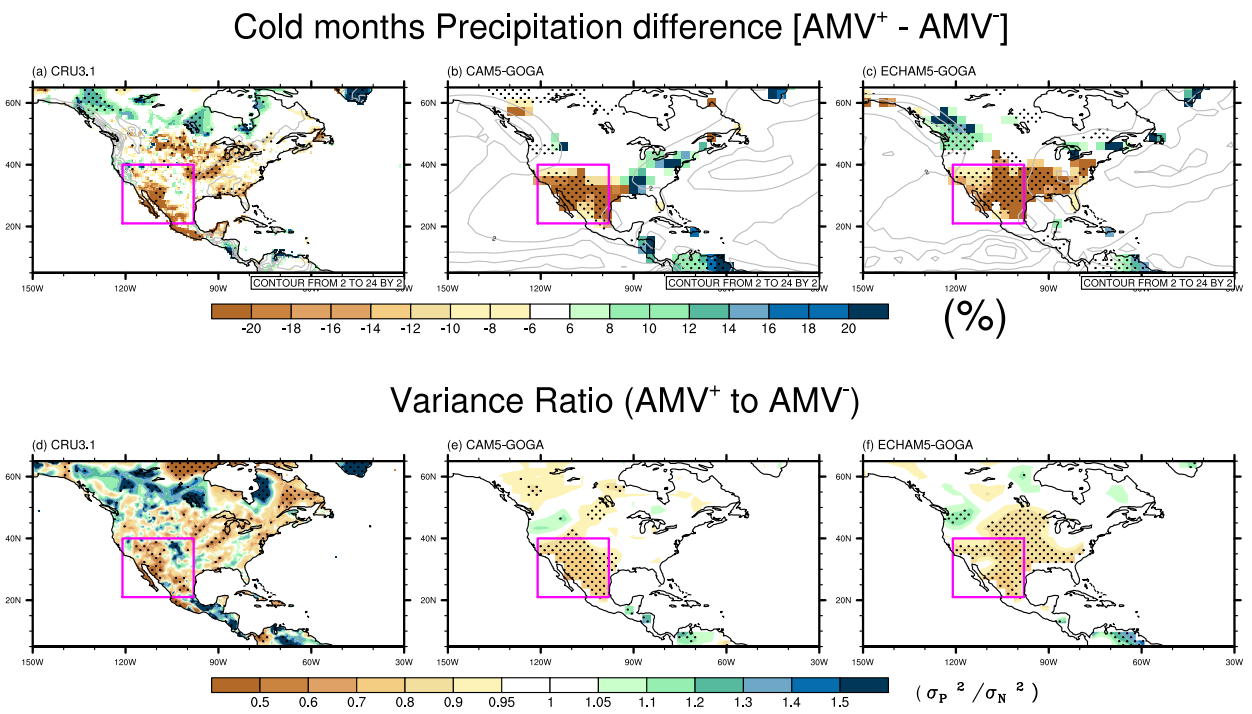

FIG. 2. (a) Observed composite difference of precipitation between AMV+ and AMV− years, in percent, with respect to the long-term mean climatology (data from CRU3.1 high-res; Harris et al. 2014). (b),(c) As in (a), but for precipitation from the (b) CAM5-GOGA and (c) ECHAM5-GOGA simulations. Overlaid in gray contours is the climatological cold season (November–April) mean precipitation. Stippling indicates areas where the difference is significant at the two-sided 95% level according to a Student's *t* test. (d) Ratio of the monthly precipitation variance for the AMV+ years to that for the AMV− years in the cold season with CRU3.1 observations and (e) that with CAM5-GOGA and (f) ECHAM5-GOGA. Stippled are the areas significant at 90% level based on a parametric F test. The SW-US in this study is defined in the magenta box. CRU3.1 and CAM5-GOGA are based on 1901–2009, but ECHAM5-GOGA is based on 1930–2013.

is anchored in the extratropical North Atlantic and extends to the tropical North Atlantic and the Gulf of Mexico, with weaker SST values in the subtropics. The temporal evolution of the AMV index is presented in Fig. 1b. Based on this time series, the years of top tercile AMV index and bottom tercile AMV index are chosen for a composite analysis.

The monthly mean observed precipitation is obtained from University of East Anglia Climate Research Unit TS3p1 data (CRU TS3p1; Harris et al. 2014) for the composite analysis conducted in the next section. The data spans from 1901 to 2009 with 1° by 1° horizontal resolution. To exclude the possible response to the radiative forcing, the linear regression onto the leading forced mode in Ting et al. (2009, 2011) is removed from the raw data.

3. AMV impact in the historical record

Observed and historical SST-forced AMV impact

Figure 2 shows the cold season (November–April) precipitation composite anomalies over the continental United States associated with the two opposite AMV phases using the century-long CRU TS3p1 data. The cold months chosen for this study are outside the season of the North American monsoon. The positive and negative years of AMV are chosen from the upper and lower terciles according to the AMV index of Ting et al. (2009) between 1930 and 2009. Statistical significance of the difference, at the 95% level, is determined using a two-sided Student's *t* test. In the SW-US and Mexico, the difference between the observed average cold-season precipitation during the years falling in the upper versus the lower tercile of the AMV index amounts up to 20% of the long-term seasonal means (Fig. 2a). The patterns in Fig. 2a are consistent with the previous study based on observations such as Ting et al. (2014, their Fig. 6a) in that they show significant dryness with the positive AMV in the SW-US, the Great Plains, and Mexico, as well as significant wetness in the Pacific Northwest and central Canada. Especially in the SW-US and Mexico, the GOGA simulations from both models (Figs. 2b and 2c) capture well the observed dryness during the positive AMV. However, the modeled

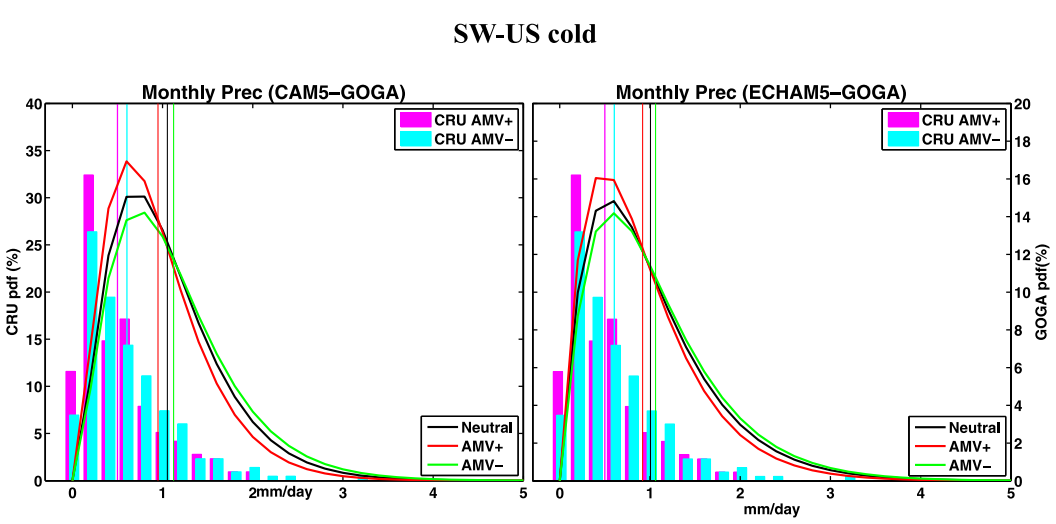

FIG. 3. (a) Probability density function (PDF) of cold season monthly precipitation in the SW-US for the AMV+ years (red), the AMV− years (green), and neutral years (black) from 16 individual CAM5-GOGA simulations. For each AMV phase, two parameters for gamma distribution are estimated using the monthly mean precipitation from all the ensemble members. The vertical line in each color indicates the mean precipitation corresponding to the curve of the same color. (b) As in (a), but for 16-member ensemble ECHAM5-GOGA. The PDF of CRU precipitation observations in the SW-US is overlaid. Magenta indicates AMV+ years and cyan indicates AMV− years.

precipitation exhibits predominant dryness over the southern United States, while the observed data do not show such significant dryness in the central south area. This disagreement can possibly be due to the internal variability of the modeled precipitation being suppressed by the ensemble average. The influence of strong internal variability on precipitation anomalies is commonly found in the modeling studies seeking SST-driven remote impacts (Schubert et al. 2016), in which ensemble mean model simulations tend to show much stronger and more spatially widespread association with the SST than does the observation (Seager and Hoerling 2014). Also, the topography of the Rocky Mountains in the coarse-resolution models could have overly simplified the spatial patterns. It is notable that AMV-related contrasts in other regions, such as the dryness in the Great Plains and the eastern United States, and the wetness in the Canadian Pacific Northwest, are captured better with EAHCM5-GOGA, but we do not discuss further the model differences, in order to focus on what the both models can capture in common.

In addition to time mean differences in precipitation, there is a notable contrast in the variance of the anomalous monthly precipitation between the two AMV phases (Figs. 2d and 2e). In particular, the variance of the monthly precipitation during the cold season in the SW-US decreases significantly during the positive AMV phase in the same area where the mean precipitation deficit occurs. The reduction in variance during the AMV positive phase relative to the negative phase is also confirmed with the CAM5-GOGA ensemble (Fig. 2d). This result suggests a role for the AMV as a modulator of the monthly mean precipitation variability in the United States, a phenomenon that has been given little attention previously. It is worth mentioning that our results in the warmer months (not shown) indicate a substantial increase of rainfall variance in the Great Plains with positive AMV phase, which is consistent with previous studies (Mo et al. 2009; Hu and Feng 2012).

To investigate further the AMV-related changes in the SW-US precipitation variability, the probability density function (pdf) for the model-simulated monthly precipitation averaged over the SW-US domain (outlined by the magenta box in Fig. 2d) is shown in Fig. 3, with a summary of the statistics presented in Table 2. Aside from the mean precipitation shift toward drier conditions in the region for positive AMV years compared to neutral and negative years, Fig. 3 indicates that drier-than-normal months occur more frequently, while wetter-than-normal months occur less frequently during positive AMV years than neutral or negative AMV years. Also, the pdf during positive AMV years exhibits a shorter right tail than during neutral or the negative AMV years, meaning that positive extremes occur less frequently during positive AMV years than negative AMV years. This contrast in the pdf is significant at the 95% level based on the Kolmogorov–Smirnov test. In Table 2, the mean difference and the variance ratio with respect to the observed precipitation

TABLE 2. Mean and monthly variance from area-averaged precipitation in the U.S. Southwest (magenta box in Fig. 2) and Niño-3.4 SST. All the variables are detrended. For CAM5-GOGA, all 16 ensemble simulations were individually included. AMV positive and negative periods are based on the upper and lower terciles of AMV amplitude calculated by Ting et al. (2009). The mean differences are presented in bold for significance at 95% with a Student's *t* test, and the monthly variance ratios are presented in bold if the variances are different at 90% significance with an F test.

	AMV mean diff		AMV variance ratio	
	SW precipitation	Niño-3.4	SW precipitation	Niño-3.4
OBS Nov–Apr	**−0.11 mm day^{-1}**	−0.04°C	0.77	**0.71**
CAM5-GOGA Nov–Apr	**−0.17 mm day^{-1}**	—	**0.73**	—
ECHAM5-GOGA Nov–Apr	**−0.14 mm day^{-1}**	—	**0.78**	—

are similar to those of the models, though not significant because of an insufficient sample size of the data. The strong agreement among the models and the observation in the changes in the AMV-related statistics indicates that additional model experiments are worthwhile.

Given the time-varying global SST in both observations and the GOGA experiments, it is difficult to determine whether the variance modulation associated with AMV as seen in Figs. 2 and 3 results entirely from the AMV SST anomalies or from the impact of SST in other ocean basins (Zhang and Delworth 2006; Li et al. 2016; Ruprich-Robert et al. 2017), particularly the tropical Pacific. It is especially difficult if there are interbasin connections between the Atlantic and the tropical Pacific. For example, a weak La Niña–like condition was found to be associated with positive AMV (see Table 2), which could result in the mean decrease of precipitation in the SW-US. Furthermore, the variance of Niño-3.4 significantly decreases during positive AMV, in the same direction as the precipitation variance in the SW-US (Table 2). Recent modeling studies have suggested that a positive phase of AMV can generate a La Niña–like pattern (Kang et al. 2014; Rupric-Robert et al. 2017). To isolate the direct impact of AMV on SW-US precipitation variability from the impact through its link with SST anomalies in other ocean basins, we perform AGCM experiments with idealized AMV SST in the North Atlantic and climatology elsewhere, which are presented in the next section.

4. AMV impact in idealized AGCM experiments

a. Impact on precipitation

To separate the directly AMV-driven differences in the means and the variances of precipitation in the United States, we analyzed the experiments forced with idealized AMV-related SST anomalies in the North Atlantic domain only. In addition to the NCAR CAM5, the ECHAM5 is used as well for more robust results. The prescribed AMV SST anomaly amplitude and spatial pattern are shown in Fig. 1a in both positive (AMV+, as shown) and negative (AMV−, obtained by multiplying the field by −1) phases.

Taking the difference between AMV+ and AMV−, both models show a significant precipitation deficit in the SW-US region during the cold season (Figs. 4a,b). ECHAM5 agrees well with CAM5 overall, except that the strength of the dryness is more severe in ECHAM5, particularly in the western United States. There are some notable disagreements with the AMV composite differences based on the CAM5-GOGA experiments (Fig. 2), possibly due to absence of historical ENSO events in the idealized experiments. The general agreement between the two independent AGCMs implies that the mean change in precipitation associated with the AMV phases in GOGA and in the observations can be driven directly by the AMV SST anomalies. In spite of the 2.5 amplification of SST forcing in the North Atlantic, the magnitude of the mean shift in SW-US in this idealized setup is less than the linearly proportional response to the forcing magnitude except in Baja California and central Mexico.

Accompanied by the decreased mean precipitation associated with AMV+, a reduction in the monthly precipitation variance is found in the SW-US, Texas/Mexico, and the central United States in both AGCMs with positive AMV SST as compared to negative AMV SST (Figs. 4c,d). The precipitation variance with AMV+ forcing can fall to about 50% of the precipitation variance with AMV− in some regions. There is an overall agreement between the two models in the variance reduction regions, although the variance reduction in ECHAM5 tends to be stronger and more widespread than that in CAM5.

The monthly precipitation probability distribution in the SW-US simulated in the fixed AMV SST experiments (Fig. 5) also agrees well with that in the GOGA experiments (Fig. 3) with both models. This agreement indicates an overall probability shift toward the drier end in monthly mean precipitation for the AMV+ experiment, and a shift toward the wetter end in the AMV− experiment. The agreement between idealized

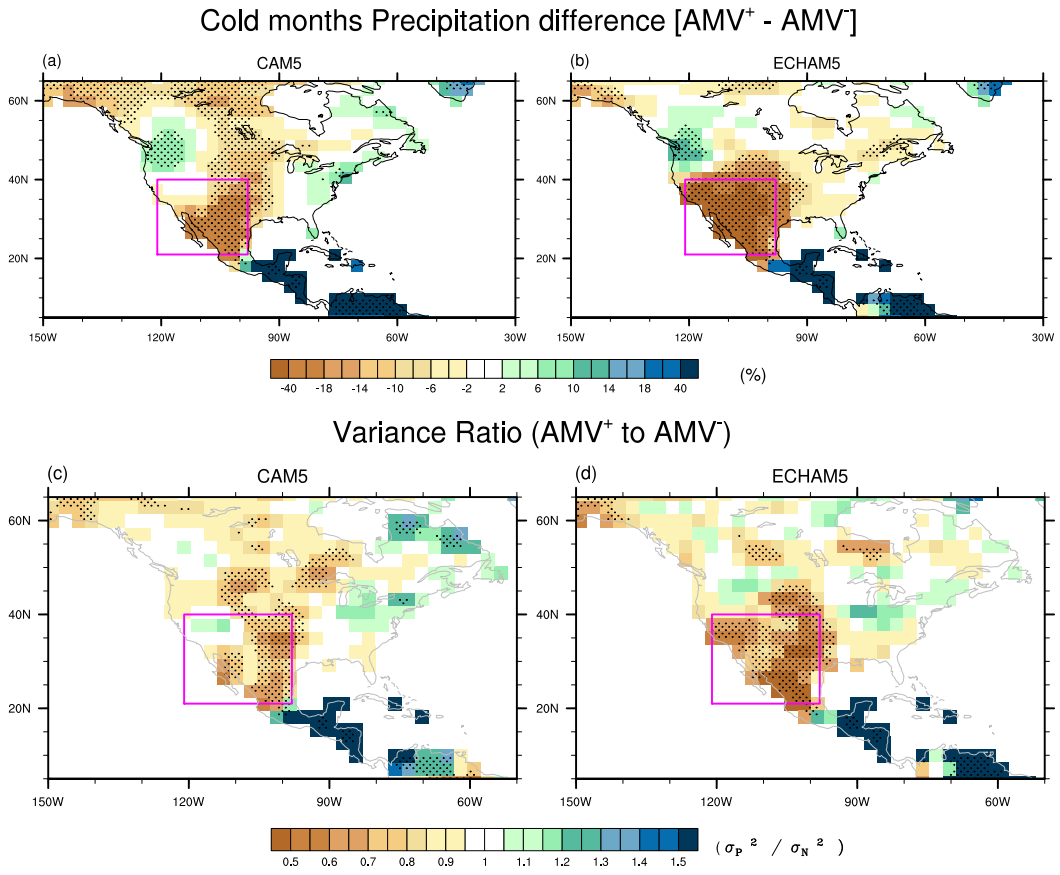

FIG. 4. (a) Mean difference between AMV+ and AMV− in percent with respect to the long-term cold season climatology in the idealized experiments with (a) CAM5 and (b) ECHAM5. Stippling indicates area significant at the 95% according to a Student's *t* test. (c) Ratio of monthly precipitation variance in cold months in AMV+ to that in AMV− with CAM5 and (d) ECHAM5 experiments. Stippling indicates areas significant at 90% according to an F test. The magenta box defines the SW-US area in this study.

AMV runs and the GOGA experiments implies that the difference between AMV phases from GOGA simulations with both models and observations is largely due to the direct influence from the AMV SST anomalies. In the idealized runs, monthly variability is due to internal atmospheric processes, while in the GOGA runs it comes from both internal atmospheric variability and SST variability in the other ocean basins, including that associated with ENSO.

To determine if the reduction in monthly precipitation variance is also detectable on a shorter time scale, such as daily variability, Fig. 6 presents the daily precipitation characteristics in terms of daily rainfall intensity and dry day occurrences. Figures 6a and 6b present the monthly mean difference between AMV+ and AMV− of the maximum daily rainfall intensity. The long-term mean climatology of the maximum daily rainfall and dry day occurrences from the control run is also shown in Fig. 6 as contours. The mean maximum daily rainfall intensity can range between 8 and 12 mm day^{-1} for the SW-US region. There can be substantial reduction in the maximum daily rainfall intensity during AMV+ as compared to AMV−, by 3 mm day^{-1} or more with ECHAM5 especially, which is one-third or more of the long-term mean value. Meanwhile, the number of dry days per month (number of days with less than 0.2 mm day^{-1} of precipitation) shows only a modest increase for AMV+ compared to the control AMV (Figs. 6c,d). Moreover, the region of prominent differences in these daily statistics coincides well with the areas where the monthly variance change is significant. Since suppression of extreme daily rainfall and increasing dry day occurrences can both contribute to reduced precipitation variability on daily time scales, this further indicates that the AMV-driven variance modulation can occur across multiple time scales. A practical inference drawn from this finding is that it is possible for AMV phases to be used as one of the predictors for seasonal probability forecasts for extreme precipitation events and persistent droughts in the SW-US.

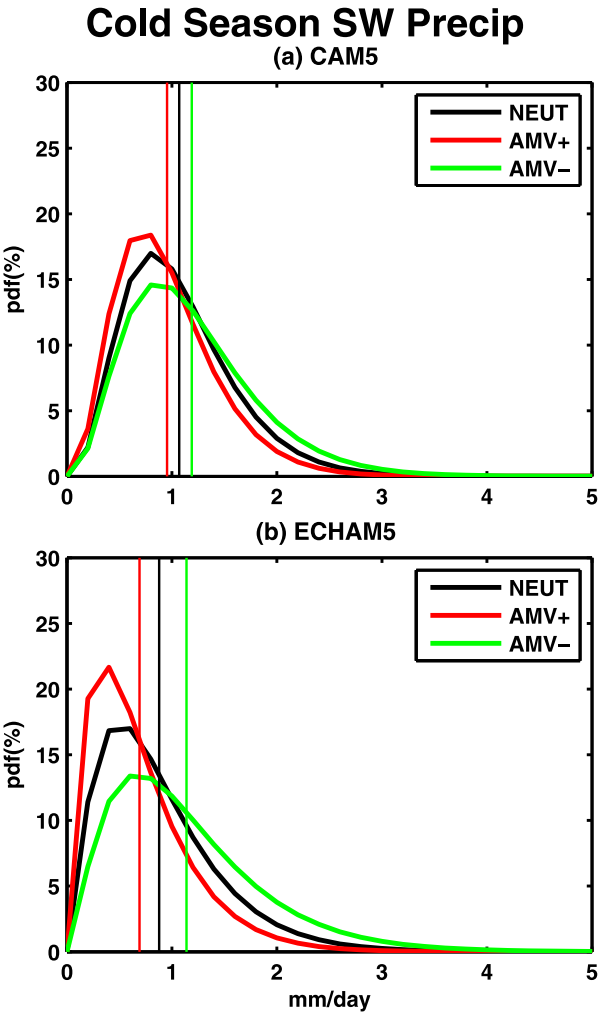

FIG. 5. As in Fig. 3, but for AMV+ (red), AMV− (green), and CTRL (black) experiments with (a) CAM5 and (b) ECHAM5.

b. *AMV impact on the atmospheric circulation*

We further examine the circulation features forced by the prescribed AMV SST anomalies by presenting, in Fig. 7, the 200-hPa geopotential height (top panels) and the sea level pressure anomalies (bottom panels) from both AGCMs for composite differences between AMV positive and negative phases. The precipitation differences between the two AMV phases are also shown as color shading in Fig. 7. Not surprisingly, there is strongly enhanced precipitation in the tropical Atlantic associated with positive AMV, particularly in the western tropical Atlantic and the Intra-American Seas (IAS) region, which also extends eastward to western Africa. In the North Atlantic, the subtropical anticyclone is weaker in the AMV+ case than in the AMV− one (Figs. 7c,d). This difference is consistent with reduced subsidence, or increased precipitation, over the subtropical Atlantic during positive AMV compared to negative AMV. Along with enhanced convection in the tropical North Atlantic, there is suppressed convection in the equatorial Pacific and a weakening of the Aleutian low (Figs. 7c,d). The upper-tropospheric responses over the Pacific and North America are remarkably similar to the negative Pacific–North American (PNA; Barnston and Livezey 1987) pattern, with an anticyclone over the Gulf of Alaska, a low over Canada, and another anticyclone across southern North America (Figs. 7a,b). The negative PNA response is consistent with the atmospheric response to a La Niña event, thus suggesting that the suppressed convection in the tropical Pacific due to positive AMV may be responsible for the circulation responses in Fig. 7. In Kushnir et al. (2010), it has been shown that a tropical North Atlantic warm SST anomaly can generate negative PNA pattern without La Niña–like SST in the tropical Pacific through a shift in the Walker circulation. This was supported by their AGCM experiments with prescribed time-varying historical SST in the tropical North Atlantic. Also, Ruprich-Robert et al. (2017) agreed with Kushnir et al. (2010) using coupled model experiments with the AMV SST restored to the observed values in the Atlantic basin.

With the same AMV SST forcing, ECHAM5 exhibits slightly stronger convection anomalies in the tropical Pacific domain than does CAM5 (Figs. 7b,d). However, the patterns of atmospheric circulation anomalies are remarkably similar in both models, which strongly suggests that these responses are robust. Additional experiments with only the tropical or the extratropical AMV SST reveal that the AMV tropical forcing alone is almost entirely responsible for the circulation and precipitation responses (not shown), again consistent with previous studies using an AGCM with sectorial historical AMV SST anomalies (Kushnir et al. 2010).

c. *AMV impact on moisture budget*

As shown in section 4a, the AMV-related changes in SST can significantly modify both the mean and the variance of the cold season precipitation in the SW-US. At the same time, there are significant changes in the atmospheric circulation associated with the AMV SST anomalies, as shown in section 4b. Here, we explore the moisture budget (Seager and Naik 2012) in both AGCMs to identify the dominant processes contributing to the precipitation variability in the SW-US and how these processes are affected by AMV. The vertically integrated moisture budget equation implies that precipitation (P) is balanced by the vertically integrated moisture convergence (MC) and moisture evaporated at the surface (E), as well as atmospheric moisture storage:

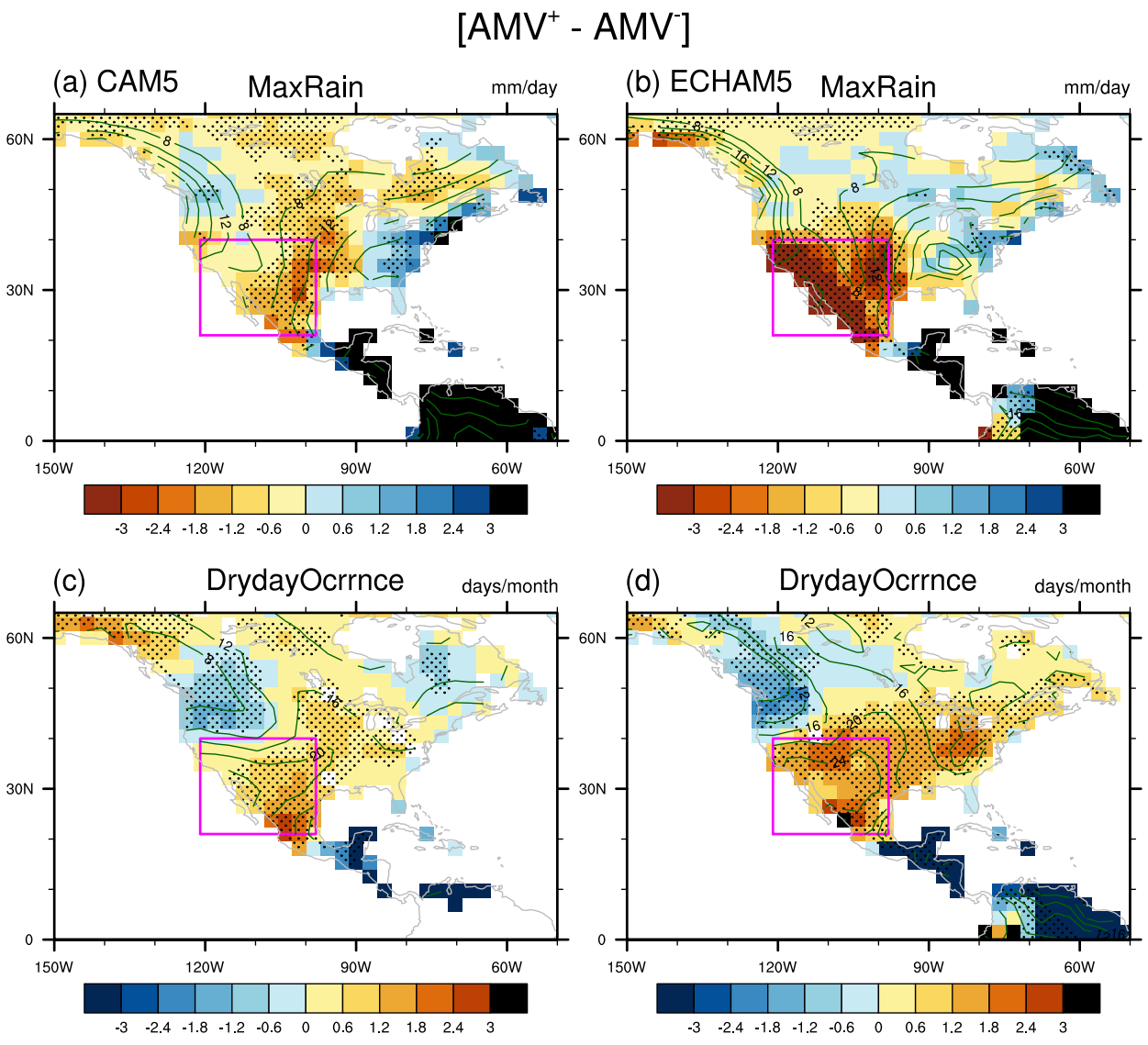

FIG. 6. Mean difference between AMV+ and AMV− in the monthly maximum of daily rainfall with (a) CAM5 and (b) ECHAM5, and in the monthly number of dry days with (c) CAM5 and (d) ECHAM5. Stippled signifies the 95% significance with a Student's t test. Contours indicate climatological mean from CTRL. The magenta box indicates the SW-US area.

$$P = -\frac{1}{g\rho_w}\int_0^{p_s} \nabla\cdot(\mathbf{u}q)\,dp + E - \frac{1}{g\rho_w}\frac{\partial}{\partial t}\int_0^{p_s} q\,dp + \varepsilon, \quad (1)$$

where q denotes specific humidity and $\mathbf{u}$ is the horizontal wind at each of the vertical levels. The error term (ε) is mainly due to the offline vertical integration and other numerical rounding errors and also likely due to errors incurred by neglecting terms associated with the tendency and convergence of condensed water not precipitated out of the column (Peixoto and Oort 1992). We first investigate the monthly mean precipitation variability during the cold season in the SW-US region and its relation to the various terms in the moisture budget equation [Eq. (1)] using the control experiment (CTRL). We find that the anomalous moisture convergence is the dominant term in the moisture budget in Eq. (1), explaining ~90%–100% of P over much of the continental U.S. area and about 80% of P variability in the SW-US, based on the linear regression relation between P and the right-hand-side terms of Eq. (1) (Table 3). Thus, we will focus mainly on the MC term in the rest of the paper. We seek the cause of the monthly precipitation anomalies in the SW-US between the two relevant subcomponents of MC anomalies as shown below:

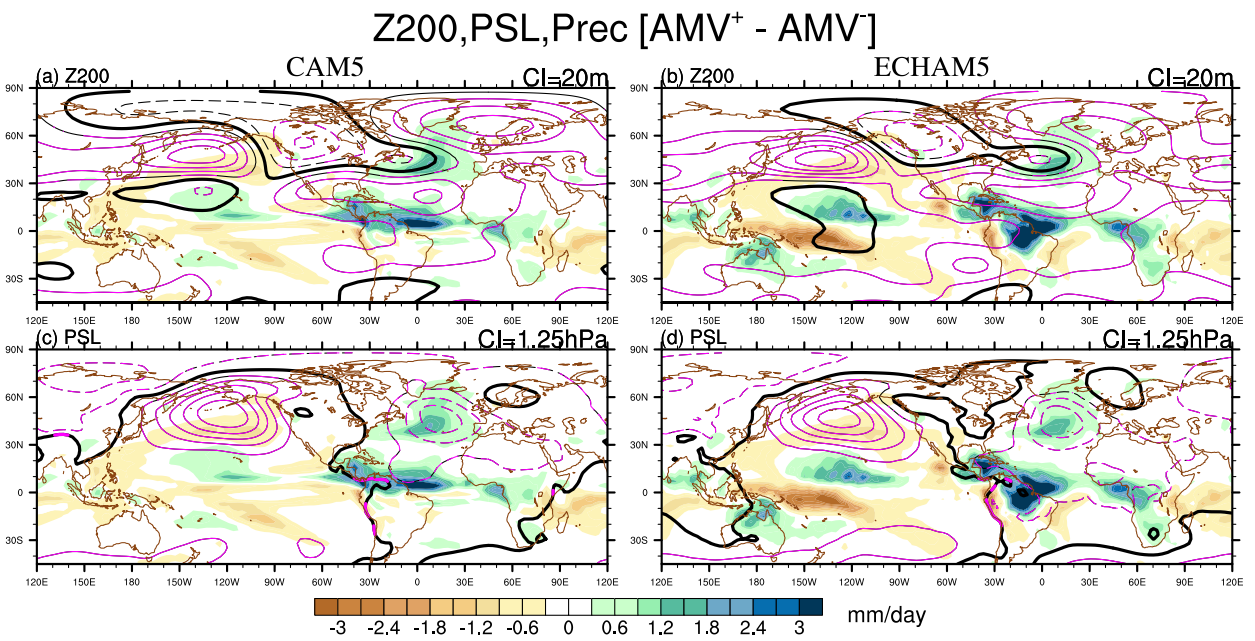

FIG. 7. Global composite differences between AMV+ and AMV− experiments. (a),(b) The geopotential height at 200 mb (CI = 20 m) in cold season with CAM5 and ECHAM5, respectively. Colored in magenta if significant at 95% with a Student's *t* test. The thinner line indicates zero, solid line indicates positive, and the dashed line indicates negative anomalies. (c),(d) As in (a),(b), but for sea level pressure (CI = 1.25 hPa). Overlaid with the precipitation difference as in Figs. 4a and 4b.

$$\mathrm{MC}'(t) = -\frac{1}{g\rho_w}\int_0^{p_{sc}} \nabla\cdot[\mathbf{u}'(t)\,q_c]\,dp - \frac{1}{g\rho_w}\int_0^{p_{sc}} \nabla\cdot[\mathbf{u}_c' q'(t)]\,dp + \mathrm{HOT}(t), \quad (2)$$

where subscript c indicates the long-term mean, and the prime indicates the monthly deviation from the long-term climatology. The first two terms in Eq. (2) represent the MC caused by anomalous circulation and that caused by anomalous column moisture, respectively, and the last term indicates the higher-order nonlinear interaction term (HOT). The separation of the first two terms is not ideal, as circulation and moisture anomalies are not strictly separable. However, it provides a framework for determining the contribution to monthly precipitation variation from moisture versus circulation fluctuations. In Fig. 8, we present maps of the correlation coefficient of the subcomponent MCs with the precipitation anomalies of the boxed area in the SW-US using the CTRL experiment. Also presented in this figure is the moisture flux caused by anomalous winds. Figure 8 shows that precipitation in the SW-US is associated with moisture flux from both the subtropical Pacific and the Gulf of Mexico, but dominated by that from the subtropical Pacific. The dominant moisture flux tends to be associated with an anomalous low center located at the West Coast of the United States causing moisture flux anomalies to converge in the SW-US and diverge near the Pacific Northwest. The MC term associated with mass circulation (shading) is positively correlated with precipitation while that due to anomalous moisture (contours) is negatively correlated with precipitation, with the total dominated by the former.

The moisture budget in Eqs. (1) and (2) above can be applied to understand the balance among the moisture terms with the changes of AMV phases using climatological

TABLE 3. Linear regression coefficients of a linear model of precipitation anomalies [*P*, left-hand side of Eq. (1)] using anomalous moisture convergence as the only independent variable [MC, the first term in the right-hand side of Eq. (1)] presented with the 95% confidence intervals. Correlation coefficients are presented in the parentheses. SW stands for the U.S. Southwest (20°–40°N, 100°–120°W), PNW stands for the Pacific Northwest (40°–50°N, 110°–120°W), GP stands for the Great Plains (35°–50°N, 95°–105°W), and SE stands for the Southeast United States (25°–35°N, 95°–78°W). Based on CTRL experiments.

	SW	PNW	GP	SE
CAM5	0.84 ± 0.044 (0.85)	0.95 ± 0.021 (0.96)	1.00 ± 0.046 (0.87)	1.16 ± 0.070 (0.82)
ECHAM5	0.82 ± 0.018 (0.97)	0.89 ± 0.014 (0.98)	0.89 ± 0.019 (0.97)	0.84 ± 0.021 (0.95)

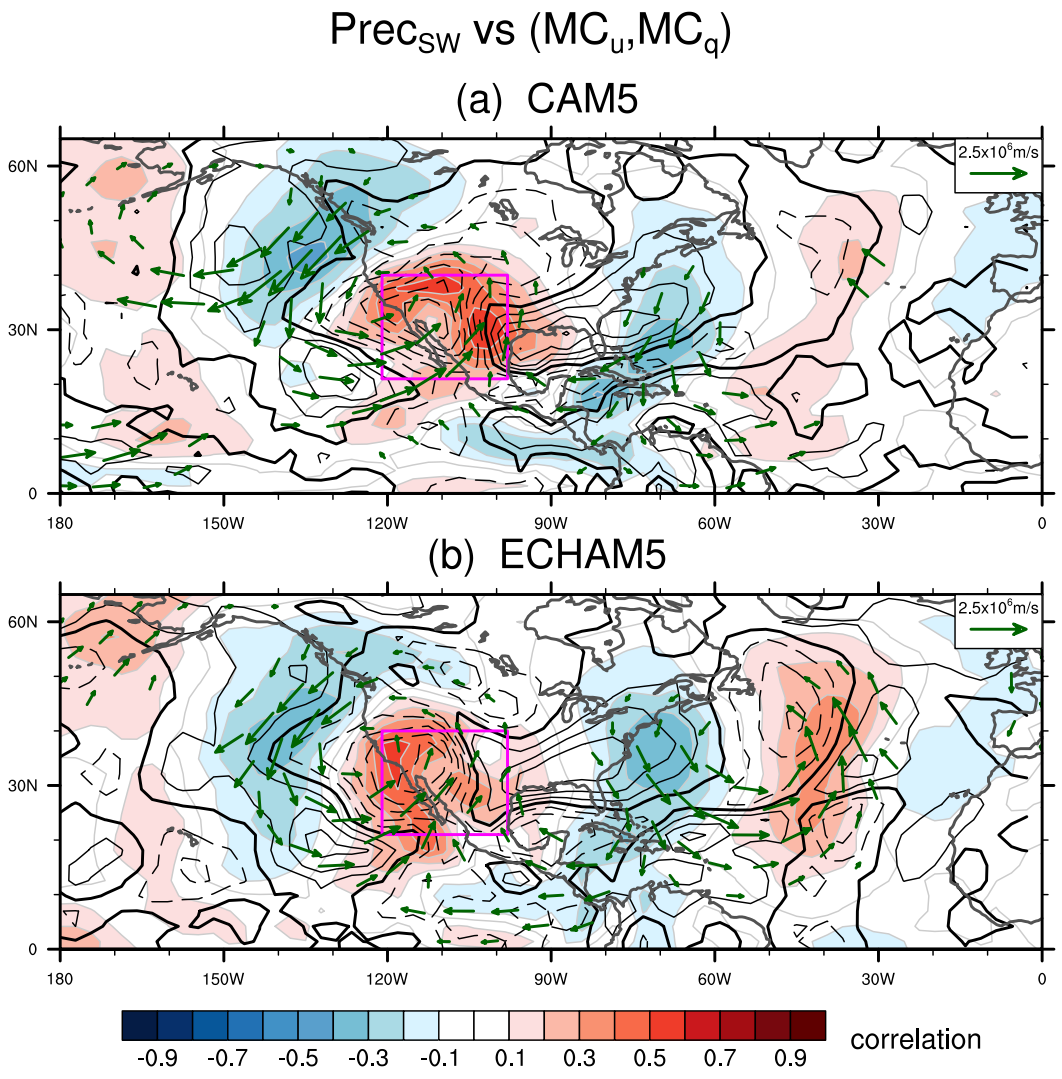

FIG. 8. Correlation coefficients with SW-US precipitation anomalies (averaged in the box) of the MC_u (shown in colored shading) and the MC_q (black line indicates contours, solid for positive, dashed for negative, and thicker for zero line, CI = 0.1), overlaid with vertically integrated moisture flux due to anomalous mass circulation (green arrows) from CTRL experiments with (a) CAM5 and (b) ECHAM5.

means of q_c and u_c from CTRL as the long-term mean and deviation of AMV+ and AMV− from CTRL as the primed variables. The relation between the precipitation change and the moisture convergence terms with respect to the difference between AMV+ and AMV− are shown in Fig. 9 for the two AGCMs. The relatively widespread drying condition during AMV+ over the southern United States and northern Mexico is largely a combination of the two MC terms, with the coastal regions dominated by the circulation-related MC and the plains as a result of changes in moisture content. Consistent with Fig. 8, the drying over SW-US is dominated by circulation changes (Figs. 9c,d), which in this case, is associated with northerly flow along the West Coast because of the anticyclone anomaly centered in the Gulf of Alaska (Fig. 7). The cyclonic anomalies over the Atlantic as shown in Fig. 7 largely contribute to the drying along the East Coast regions where the flow is northerly or northwesterly, which fluxes low mean moisture into the region. The circulation-related changes in moisture convergence (Figs. 9c,d) is also consistent with the suppressed vertical motion shown in Figs. 10a and 10b. The MC term involving moisture content change (Figs. 9e,f), on the other hand, is determined by both the specific humidity difference between AMV positive and negative phases, and the climatological mass divergence (Figs. 10a,b). Because of the decrease in specific humidity across the domain of

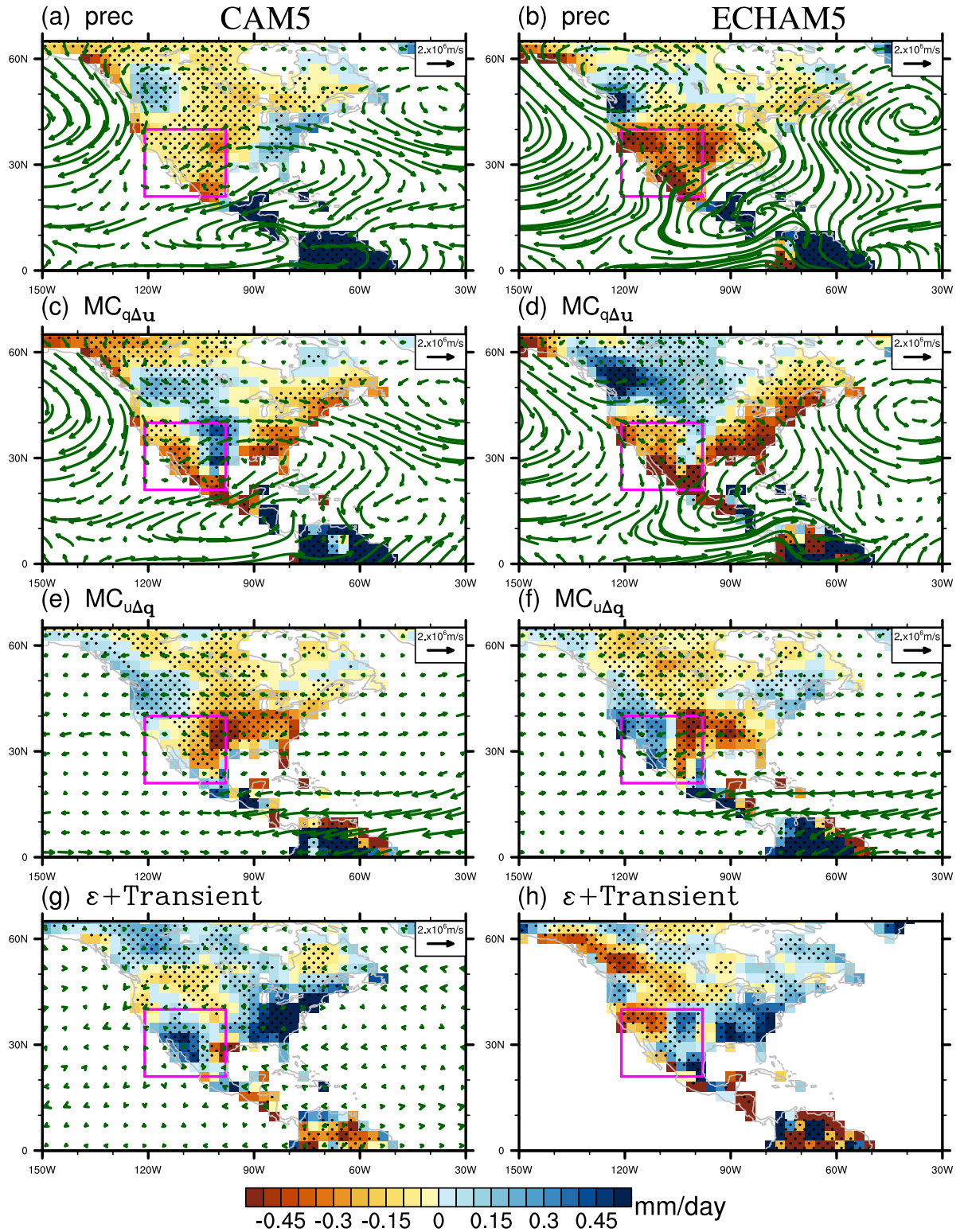

FIG. 9. Difference between AMV+ and AMV− for (a),(b) precipitation overlaid with the moisture flux vectors; (c),(d) moisture convergence (MC) due to difference in mass circulation; (e),(f) MC due to difference in column moisture content; and (g),(h) error [ε in Eq. (1)] and MC by transient eddies, overlaid with the corresponding subcomponent moisture flux vectors with CAM5 and ECHAM5, respectively. Stippling indicates the area significant at 95% according to a Student's t test. The moisture flux vectors are based on the monthly product. Magenta box indicates the SW-US area.

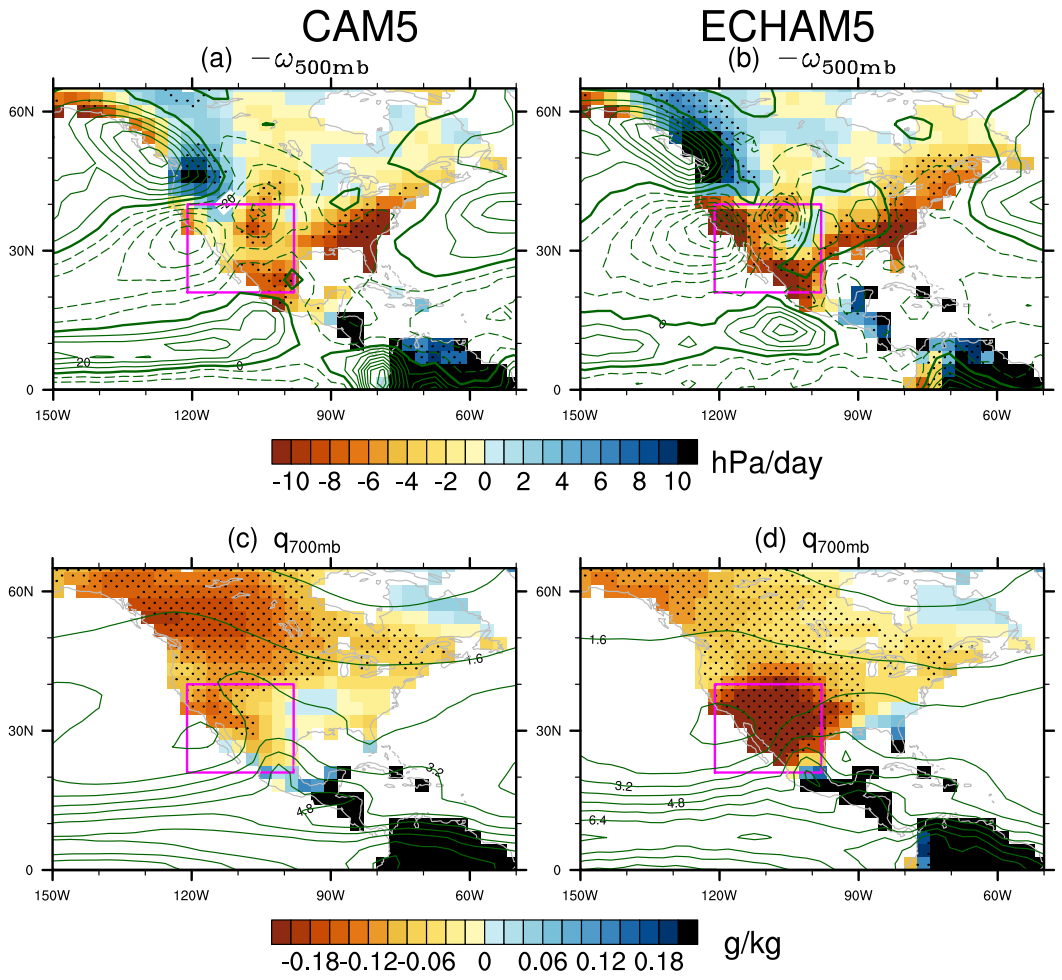

FIG. 10. Difference between AMV+ and AMV− for (a),(b) cold season vertical pressure velocity (positive upward) at 500 hPa with the climatological mean from CTRL overlaid in green contours with CAM5 and ECHAM5, respectively. (c),(d) As in (a),(b), but for specific humidity at 700 mb. Dashed lines indicate negative values, solid lines indicate positive values, and thicker lines are zero contour lines. Contour interval for the climatological values is 10 hPa day^{-1} for pressure velocity, and 0.8 g kg^{-1} for specific humidity. Stippling indicates that the mean difference between AMV+ and AMV− is significant at 95%.

interests (Figs. 10c,d), there would be reduced moisture convergence where the mean mass flow converges, while there would be increased moisture convergence where the mean mass flow diverges. This is more clearly shown in Fig. 9f for the ECHAM5 model with an east–west dipole over the southern part of United States. Both models show that transient eddies are important in the East Coast of the United States, but less so in the Southwest (Figs. 9g,h). Because of data availability, the error (ε) with ECHAM5 is not separable from the MC by transients. To determine why the monthly precipitation variance is suppressed in AMV+ as compared to AMV−, we compare the variance of the relevant terms between the two AMV phases in the moisture budget. We first construct the monthly time series of the moisture convergence terms. These include steady monthly mean moisture convergence $\left[\mathrm{MC}_{uq}(t) = -(1/g\rho_w)\int \nabla \cdot \overline{\mathbf{u}(t)}\,\overline{q(t)}\,dp\right]$, where the bar represents monthly mean, the moisture convergence due to monthly variations of the wind component $\left[\mathrm{MC}_{u}(t) = -(1/g\rho_w)\int \nabla \cdot \overline{\mathbf{u}(t)}\,\overline{q_c}\,dp\right]$, where the subscript c means long-term mean, and the moisture convergence due to monthly variations of the moisture content $\left[\mathrm{MC}_{q}(t) = -(1/g\rho_w)\int \nabla \cdot \overline{\mathbf{u}}_c\overline{q(t)}\,dp\right]$, for the two AMV phases. For this calculation, the long-term monthly mean of the wind or specific humidity are obtained from the corresponding AMV experiments. Once we obtain the monthly time series for these moisture convergences at each grid point, the variance and variance ratio between AMV+ and AMV− can be calculated. The contribution from submonthly time-scale eddies is derived as a residual for each month between $P - E$ and MC_{uq}.

Figure 11 shows the variance ratio of the various moisture budget terms, including $P - E$, E, total monthly mean, and submonthly transient moisture convergences for ECHAM5 only. The pattern with CAM5 broadly agrees with these plots with a somewhat weaker signal and less statistical significance (not shown). Compared to the precipitation variance ratio in Figs. 4c and 4d, it is clear that there is a similar reduction in variance for AMV positive phase in precipitation minus evaporation (Fig. 11a), while the difference in variance between AMV+ and AMV− in evaporation is relatively small. The $P - E$ variance ratio is largely explained by the monthly mean moisture convergence term (Fig. 11c), with nonnegligible contribution from the transient component (Fig. 11d). Note that the variance and variance ratio calculations here are not linear, thus one cannot add Figs. 11c and 11d to get the total in Fig. 11a. One can infer from this separation, however, that the precipitation variance is suppressed in AMV+ compared with AMV− because of suppressed variance in both the monthly mean and submonthly transient moisture convergences, consistent with Figs. 5 and 6. The reduction in monthly mean moisture convergence variance in AMV+ seems to be dominated by the dynamic MC term (i.e., the moisture convergence due to circulation variations, MC_u, Fig. 11e), with little contribution from the term involving monthly mean variations of q (Fig. 11f). The dynamic moisture convergence variations will display a small range of variability if the column moisture content (q_c) is reduced or if vertical movement of the air masses becomes less active (reduced mass convergence or vertical motion). During the positive AMV phase, precipitation amounts vary less, partly because there is suppressed vertical motion (Fig. 10b) and partly because there is overall lower column moisture content to be condensed into rain when there is low-level mass convergence (Fig. 10d). These two processes combine to reduce the AMV+ variance in precipitation and MC as compared to AMV−. In forming such variance ratio of MC_u the relative importance between these two factors, column moisture content change and modulated vertical motion variability, can be further assessed by the ratio of squared mean column moisture and the variance ratio of vertical motion (Figs. 11g and 11h). From these estimates, it is shown that the shift in mean column moisture content plays a more important role in modulating MC_u variance for ECHAM5, whereas the modulated upward motion variability plays an equally important role for CAM5 (not shown). Additional analyses to further define the relative importance of the background column moisture versus the upward motion variability are not pursued, as it is highly dependent on the individual choice of the model physics schemes.

In Fig. 12, we examine the ambient physical conditions, which can possibly be associated with suppressed vertical motion and reduced low-level moisture in AMV+ compared to AMV−. These conditions are shown in longitude–pressure cross sections averaged over the latitudes from 20° to 40°N, for temperature and vertical motion in the top panels, and specific humidity and meridional wind in the bottom panels, for the longitude band from the eastern Pacific coast to the Atlantic. When AMV is in its positive phase, more moisture evaporates because of a warmer ocean surface in the Gulf of Mexico and the tropical Atlantic (Figs. 12c,d). The increased moisture rises with convection and turns into precipitation aloft as shown in Fig. 7; thus, more latent heat is released at the upper level. In the meantime, the upper-level anticyclonic circulation anomaly redistributes the heating toward the United States from the tropical Atlantic and forms a geostrophic balance with the upper-level height gradient associated with the warming (Figs. 7a,b; Figs. 12a,b). ECHAM5 generates stronger upper-level warming (Fig. 12b) than CAM5 (Fig. 12a), as it produces more precipitation than CAM5 over the tropical Atlantic (Figs. 7a,b). The upper-tropospheric warming increases the static stability, which, we suspect, suppresses vertical motion over the North American land region. On the other hand, we believe that the northerly flow along the West Coast of the United States (Figs. 12c,d) can be associated with lower specific humidity over a large part of the United States in the lower troposphere. Both of these processes suggest reduction in the mean and the short-term variability of precipitation over the land region, particularly over the SW-US.

5. Summary and discussion

In this study, we have examined the influence of the AMV on precipitation characteristics in the SW-US, in particular its modulation of shorter-term variability. To separate the AMV-driven effects, we first showed the contrast in cold season mean precipitation and the monthly variance between the two opposite AMV phases in the observed precipitation record. Then, using atmospheric general circulation model experiments with prescribed global observed historical SST using the CAM5 and ECHAM5 models, we show that the precipitation contrasts associated with AMV, which we detected in the observations, can be simulated with the (prescribed) global historical SST conditions. Moreover, two idealized experiments with two different AGCMs, in which prescribed positive and negative AMV SST

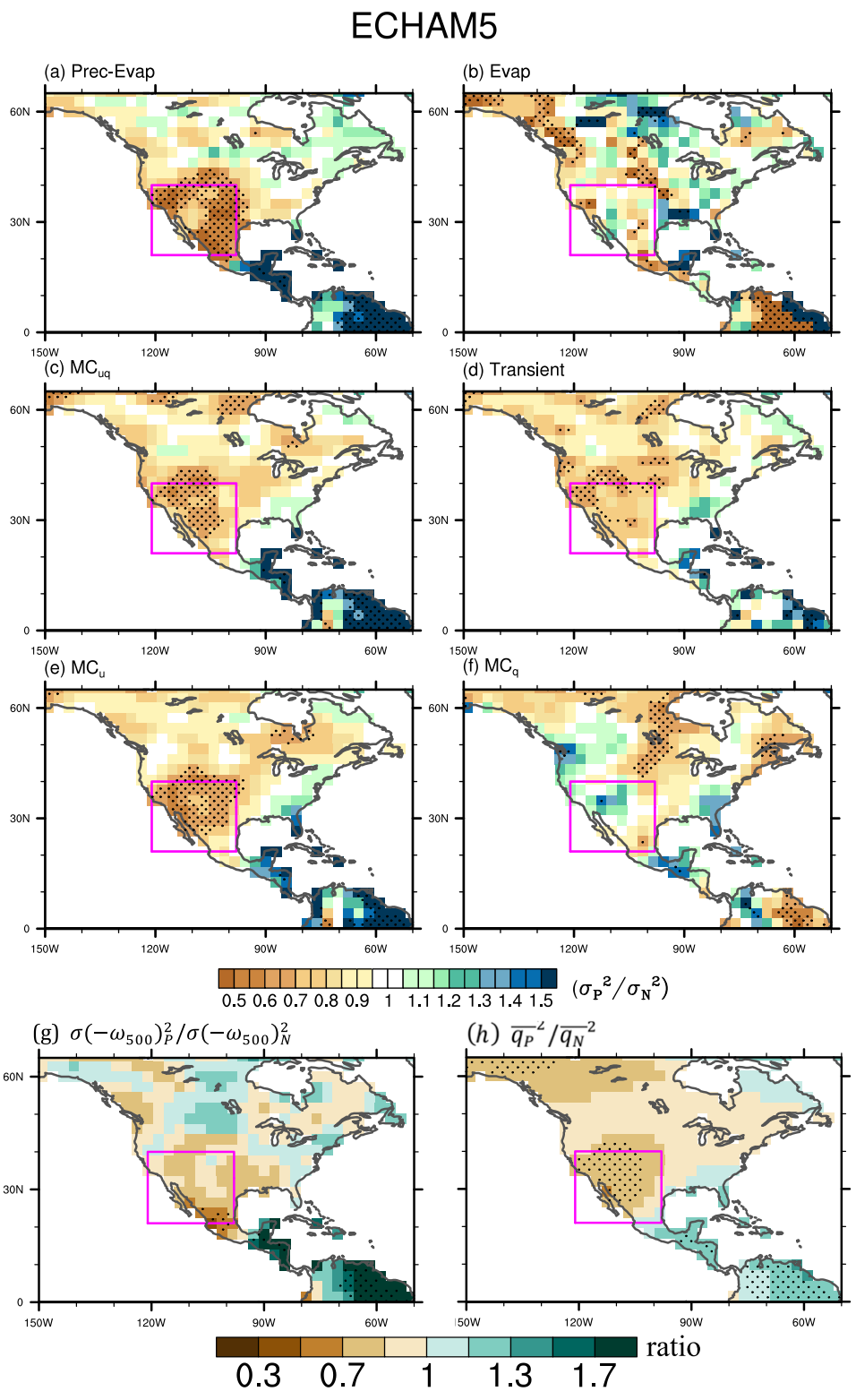

FIG. 11. Variance ratio of AMV+ to AMV− for (a) precipitation minus evaporation, (b) evaporation, (c) monthly moisture convergence (MC), (d) MC due to transient eddies, (e) monthly MC due to mass circulation anomalies, (f) monthly MC due to column moisture anomalies, and (g) pressure velocity, all with ECHAM5. Stippling indicates significance at 90% according to an F test. (h) Ratio of mean column moisture content squared. Stippling indicates that the mean difference between AMV+ and AMV− is significant at 95%. Magenta box indicates the SW-US area.

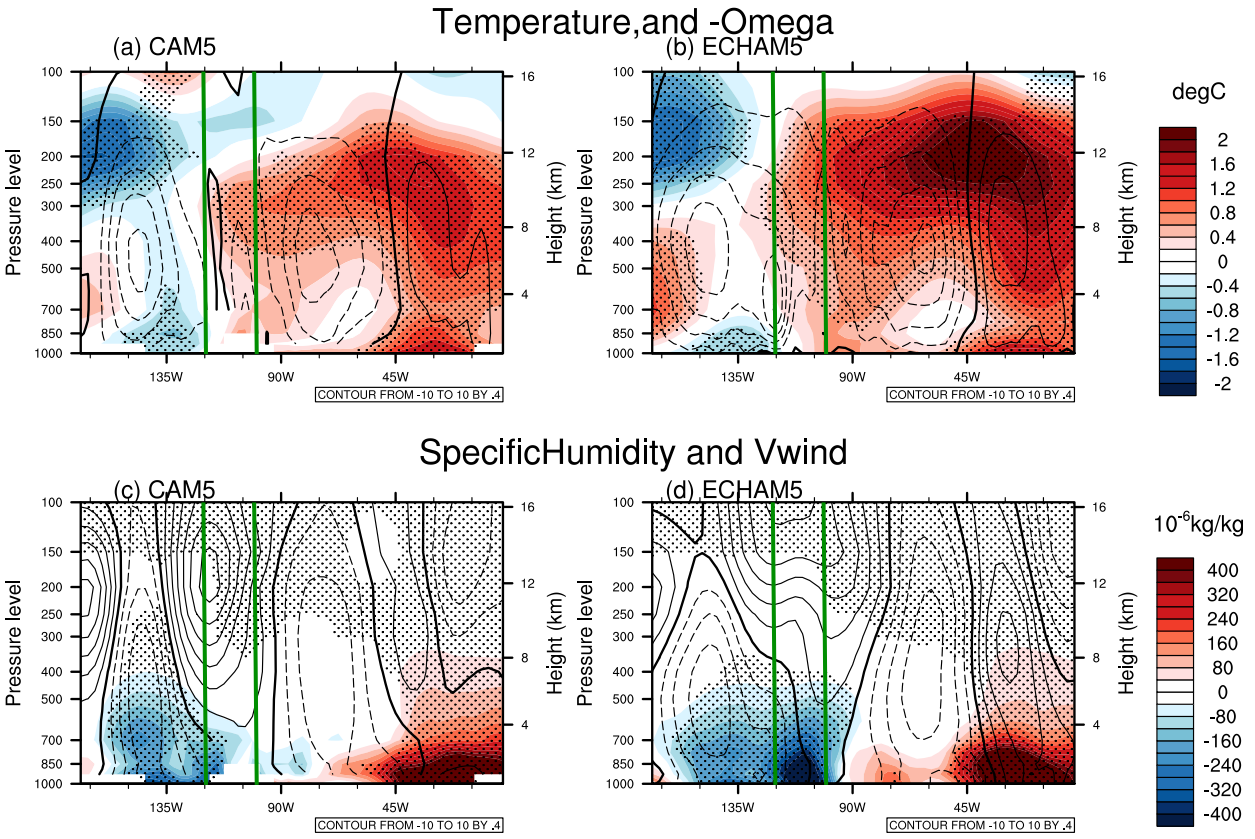

FIG. 12. Pressure–longitude plane cross section averaged between 20° and 40°N for difference between AMV+ and AMV− experiments in temperature, shown by shading, and upward vertical pressure velocity contoured in black (hPa s^{-1}, CI = 0.4) with (a) CAM5 and (b) ECHAM5. (c),(d) As in (a),(b), but for specific humidity in shading and meridional wind velocity contoured in black (m s^{-1}, CI = 0.4). Stippling indicates that the difference is significant at 95% with a Student's *t* test. Two green vertical lines indicate the longitude range covering the SW-US area.

anomaly patterns were confined to only the North Atlantic, confirmed that the precipitation variance in the continental United States could be significantly affected by the AMV-related SST anomalies.

The atmospheric circulation responses to AMV forcing are very similar between the two independent GCMs, consisting of a negative Pacific–North American pattern with an anticyclone over the Gulf of Alaska, a cyclone in northern Canada, and another anticyclone in the southern part of North America. The reduction in storm activity and the reduced moisture divergence due to mean flow divergence appear to be connected with the mean reduction in precipitation during the AMV positive phase. The source of the model dependence in the spatial pattern and magnitude of the precipitation variance change seems to be the model-dependent physics schemes, as the circulation anomaly patterns from two models strikingly resemble each other. The moisture budget analysis suggests in further detail that the rainfall variance reduction with AMV+ can be explained by moisture convergence caused by reduced variability in mass circulation. In addition, the reduction in the background moisture with AMV+ reinforces the precipitation variance reduction. However, the relative roles of these two factors in generating such variance reduction with AMV+ are quite different between the two models. With ECHAM5, reduction of background moisture plays a more important role, whereas both play equally important roles with CAM5. The model dependence is detected in each model's preference in rainfall types. As we separate the precipitation into large-scale and convective components, we find out that large-scale precipitation, which is related to the column humidity, dominates ECHAM5 precipitation (comprising more than 80% of the total monthly rainfall) in the SW-US, whereas convective precipitation due to local updraft is also remarkably important for CAM5 precipitation (about 40% of total precipitation) in the SW-US.

We propose the following plausible mechanisms for the reduction in both the mean precipitation and monthly precipitation variance during AMV+ as compared to AMV−. During the AMV positive phase,

warmer SST in the tropical Atlantic shifts the ITCZ northward and enhances convection in the tropical North Atlantic and the IAS, which then warms the tropical upper troposphere locally and also extends to the North American continents. The enhanced upper-tropospheric warming in turn leads to enhanced static stability and reduces vertical motion over the continental United States. The suppression of vertical motion not only causes the mean drying, but also reduces precipitation variability. The southwestern United States is further impacted by the anticyclone centered over the Gulf of Alaska and a generally La Niña–like circulation response that favors northerly flow along the West Coast, which advects drier air from the north.

The remarkable similarity between the two models in generating a La Niña–like circulation response over the Pacific and North American region during the AMV positive phase is worth further study. This has been shown before using a slightly different model setting (Kushnir et al. 2010) and using a coupled model with restoring AMV SST (Ruprich-Robert et al. 2017). Further diagnostics using a simple linear model may be helpful, as shown in Kushnir et al. (2010).

This study is the first attempt to test the hypothesis that there is a direct AMV-driven modulation of precipitation variability in the continental United States. This study does not provide a quantitative assessment of the observed differences between the opposite AMV phases and whether these are directly AMV driven. The monthly precipitation variance in the idealized AMV experiments is due to the random weather perturbation, preconditioned on the permanent AMV-SST forcing in the North Atlantic. We have not investigated if ENSO strength or the strength of its impact over the continental United States is modulated by AMV. Kang et al. (2014) and others have shown, using coupled GCM experiments, indications of AMV modulation of ENSO itself. To be able to quantitatively separate the observed variance ratio between indirect and direct influences of AMV on ENSO, we need a new set of experiments with historical SST anomalies as in Kushnir et al. (2010).

Acknowledgments. We thank the three reviewers for their valuable comments that helped to improve the manuscript. This work was supported by the National Oceanographic and Atmospheric Administration through Grant NA10OAR4310223 and the National Science Foundation through Grant AGS-1243204.

REFERENCES

Allen, M. R., and L. A. Smith, 1997: Optimal filtering in singular spectrum analysis. *Phys. Lett.*, **234**, 419–428, https://doi.org/10.1016/S0375-9601(97)00559-8.

Barnston, A. G., and R. E. Livezey, 1987: Classification, seasonality and persistence of low-frequency atmospheric circulation patterns. *Mon. Wea. Rev.*, **115**, 1083–1126, https://doi.org/10.1175/1520-0493(1987)115<1083:CSAPOL>2.0.CO;2.

Enfield, D. B., A. M. Mestas-Nunez, and P. J. Trinble, 2001: The Atlantic Multidecadal Oscillation and its relation to rainfall and river flows in the continental US. *Geophys. Res. Lett.*, **28**, 2077–2080, https://doi.org/10.1029/2000GL012745.

Guo, Y., M. Ting, Z. Wen, and D. E. Lee, 2017: Distinct patterns of tropical Pacific SST anomaly and their impacts on North American climate. *J. Climate*, **30**, 5221–5241, https://doi.org/10.1175/JCLI-D-16-0488.1.

Harris, I., P. D. Jones, T. J. Osborn, and D. H. Lister, 2014: Updated high-resolution grids of monthly climatic observations—The CRU TS3.10 dataset. *Int. J. Climatol.*, **34**, 623–642, https://doi.org/10.1002/joc.3711.

Holland, M. M., D. A. Bailey, B. P. Briegleb, B. Light, and E. Hunke, 2012: Improved sea ice shortwave radiation physics in CCSM4: The impact of melt ponds and aerosols on Arctic Sea ice. *J. Climate*, **25**, 1413–1430, https://doi.org/10.1175/JCLI-D-11-00078.1.

Howitt, R. E., J. Medellin-Azuara, D. MacEqan, J. Lund, and D. Sumner, 2014: Economic analysis of the 2014 drought for California agriculture. Center for Watershed Sciences, University of California, 20 pp., https://watershed.ucdavis.edu/files/biblio/DroughtReport_23July2014_0.pdf.

Hu, Q., and S. Feng, 2012: AMO- and ENSO-driven summertime circulation and precipitation variations in North America. *J. Climate*, **25**, 6477–6495, https://doi.org/10.1175/JCLI-D-11-00520.1.

——, ——, and R. J. Oglesby, 2011: Variations in North American summer precipitation driven by the Atlantic multidecadal oscillation. *J. Climate*, **24**, 5555–5570, https://doi.org/10.1175/2011JCLI4060.1.

Huang, B. and Coauthors, 2015: Extended Reconstructed Sea Surface Temperature version 4 (ERSSTv4). Part I: Upgrades and intercomparisons. *J. Climate*, **28**, 911–930, https://doi.org/10.1175/JCLI-D-14-00006.1.

Jong, B.-T., M. Ting, R. Seager, N. Henderson, and D. E. Lee, 2018: Role of equatorial Pacific SST forecast error in the late winter California precipitation forecast for the 2015/16 El Niño. *J. Climate*, **31**, 839–852, https://doi.org/10.1175/JCLI-D-17-0145.1.

Kang, I. S., H.-H. No, and F. Kucharski, 2014: ENSO amplitude modulation associated with the mean SST changes in the tropical central Pacific induced by Atlantic multidecadal oscillation. *J. Climate*, **27**, 7911–7920, https://doi.org/10.1175/JCLI-D-14-00018.1.

Knight, J. R., C. K. Folland, and A. A. Scaife, 2006: Climate impacts of the Atlantic Multidecadal Oscillation. *Geophys. Res. Lett.*, **33**, L17706, https://doi.org/10.1029/2006GL026242.

Kushnir, Y., R. Seager, M. Ting, N. Naik, and J. Nakamura, 2010: Mechanisms of tropical Atlantic SST influence on North American precipitation variability. *J. Climate*, **23**, 5610–5618, https://doi.org/10.1175/2010JCLI3172.1.

Li, X., S. P. Xie, S. T. Gille, and C. Yoo, 2016: Atlantic-induced pan-tropical climate change over the past three decades. *Nat. Climate Change*, **6**, 275–279, https://doi.org/10.1038/nclimate2840.

McCabe, G. J., M. A. Palecki, and J. L. Betancourt, 2004: Pacific and Atlantic Ocean influences on multidecadal drought frequency in the United States. *Proc. Natl. Acad. Sci. USA*, **101**, 4136–4141, https://doi.org/10.1073/pnas.0306738101.

Mo, K., J.-K. Schemm, and S.-H. Yoo, 2009: Influence of ENSO and the Atlantic multidecadal oscillation on drought over the

United States. *J. Climate*, **22**, 5962–5982, https://doi.org/10.1175/2009JCLI2966.1.

Neale, R. B., J. Richter, S. Park, P. H. Lauritzen, S. J. Vavrus, P. J. Rasch, and M. Zhang, 2013: The mean climate of the Community Atmosphere Model (CAM4) in forced SST and fully coupled experiments. *J. Climate*, **26**, 5150–5168, https://doi.org/10.1175/JCLI-D-12-00236.1.

Notaro, M., Z. Liu, R. G. Gallimore, J. W. Williams, D. S. Gutzler, and S. Collins, 2010: Complex seasonal cycle of ecohydrology in the Southwest United States. *J. Geophys. Res.*, **115**, G04034, https://doi.org/10.1029/2010JG001382.

Oleson K.W., and Coauthors, 2013: Technical description of version 4.5 of the Community Land Model (CLM). NCAR/TN-503+STR, 434 pp., www.cesm.ucar.edu/models/cesm1.2/clm/CLM45_Tech_Note.pdf.

Peixoto, J. P., and A. H. Oort, 1992: *Physics of Climate*. Springer-Verlag, 520 pp.

Pomposi, C., A. Giannini, Y. Kushnir, and D. E. Lee, 2016: Understanding Pacific Ocean influence on interannual precipitation variability in the Sahel. *Geophys. Res. Lett.*, **43**, 9234–9242, https://doi.org/10.1002/2016GL069980.

Roeckner, E., and et al, 2003: The atmospheric general circulation model ECHAM5, Part I. Max Planck Institut für Meteorologie, Rep. 349, 140 pp., https://www.mpimet.mpg.de/fileadmin/publikationen/Reports/max_scirep_349.pdf.

Rogers, J. C., and J. S. M. Coleman, 2003: Interactions between the Atlantic Multidecadal Oscillation, El Niño/La Niña, and the PNA in winter Mississippi Valley stream flow. *Geophys. Res. Lett.*, **30**, 1518, https://doi.org/10.1029/2003GL017216.

Ruprich-Robert, Y., R. Msadek, F. Castruccio, S. Yeager, T. Delworth, and G. Danabasoglu, 2017: Assessing the climate impacts of the observed Atlantic multidecadal variability using the GFDL CM2.1 and NCAR CESM1 global coupled models. *J. Climate*, **30**, 2785–2810, https://doi.org/10.1175/JCLI-D-16-0127.1.

Schubert, S. D., M. J. Suarez, P. J. Pegion, R. D. Koster, and J. T. Bacmeister, 2004: Causes of long-term drought in the U.S. Great Plains. *J. Climate*, **17**, 485–503, https://doi.org/10.1175/1520-0442(2004)017<0485:COLDIT>2.0.CO;2.

——, and Coauthors, 2016: Global meteorological drought: A synthesis of current understanding with a focus on SST drivers of precipitation deficits. *J. Climate*, **29**, 3989–4019, https://doi.org/10.1175/JCLI-D-15-0452.1.

Schulz, J., L. Dümenil, and J. Polcher, 2001: On the land surface–atmosphere coupling and its impact in a single-column atmospheric model. *J. Appl. Meteor.*, **40**, 642–663, https://doi.org/10.1175/1520-0450(2001)040<0642:OTLSAC>2.0.CO;2.

Seager, R., and N. Naik, 2012: A mechanisms-based approach for detecting recent anthropogenic hydroclimate change. *J. Climate*, **25**, 236–261, https://doi.org/10.1175/JCLI-D-11-00056.1.

——, and M. Hoerling, 2014: Atmosphere and ocean origins of North American droughts. *J. Climate*, **27**, 4581–4606, https://doi.org/10.1175/JCLI-D-13-00329.1.

——, ——, S. Schubert, H. Wang, B. Lyon, A. Kumar, J. Nakamura, and N. Henderson, 2015: Causes of the 2011–14 California drought. *J. Climate*, **28**, 6997–7024, https://doi.org/10.1175/JCLI-D-14-00860.1.

Sewall, J. O., and L. C. Sloan, 2004: Disappearing Arctic sea ice reduces available water in the American west. *Geophys. Res. Lett.*, **31**, L06209, https://doi.org/10.1029/2003GL019133.

Sheppard, P. R., A. C. Comrie, G. D. Packin, K. Angersbach, and M. K. Hughes, 2002: The climate of the US Southwest. *Climate Res.*, **21**, 219–238, https://doi.org/10.3354/cr021219.

Simmons, A. J., and D. M. Burridge, 1981: An energy and angular-momentum conserving vertical finite difference scheme and hybrid vertical coordonates. *Mon. Wea. Rev.*, **109**, 758–766, https://doi.org/10.1175/1520-0493(1981)109<0758:AEAAMC>2.0.CO;2.

Sutton, R. T., and D. L. Hodson, 2005: Atlantic Ocean forcing of North American and European summer climate. *Science*, **309**, 115–118, https://doi.org/10.1126/science.1109496.

Ting, M., Y. Kushnir, R. Seager, and C. Li, 2009: Forced and internal twentieth-century SST trends in the North Atlantic. *J. Climate*, **22**, 1469–1481, https://doi.org/10.1175/2008JCLI2561.1.

——, ——, ——, and L. Cuihua, 2011: Robust features of Atlantic multi-decadal variability and its climate impacts. *Geophys. Res. Lett.*, **38**, L17705, https://doi.org/10.1029/2011GL048712.

——, ——, and C. Li, 2014: North Atlantic Multidecadal SST Oscillation: External forcing versus internal variability. *J. Mar. Syst.*, **133**, 27–38, https://doi.org/10.1016/j.jmarsys.2013.07.006.

Titchner, H. A., and N. A. Rayner, 2014: The Met Office Hadley Centre sea ice and sea surface temperature data set, version 2: 1. Sea ice concentrations. *J. Geophys. Res.*, **119**, 2864–2889, https://doi.org/10.1002/2013JD020316.

Zhang, R., and T. L. Delworth, 2006: Impact of the Atlantic multidecadal oscillation on North Pacific climate variability. *Geophys. Res. Lett.*, **33**, L17712, https://doi.org/10.1029/2006GL026267.